Journal of Engineering and Technological Advances (JETA)
https://jeta.segi.edu.my/index.php/segi
2024 Vol. 10 No. 2

THE EFFECT OF WELDING METHODS ON THE MECHANICAL AND MICROSTRUCTURE OF HIGH-CARBON STEEL

[1]Omiogbemi, I.M.B.*, [1]Awode, E.I., [2]Okwum, C., [1]Olatunji, E.C., [3]Inobeme, F.O., [1]Awopetu, G.A., [1]Awwal K.S., [4]Dagwa, M.I., [5]Olaiya, K.A.

[1] Mechanical Engineering Department, Air Force Institute of Technology, 800282, Kaduna, Nigeria.

[2] Mechanical Engineering Unit, Niger State Ministry of Works, State Secretariat, 920101, Minna, Niger State.

[3] Mechanical and Aerospace Ground Engineering Department, Air Force Institute of Technology, 800282, Kaduna, Nigeria.

[4] Mechanical Engineering Department, University of Abuja, Gwagwalada, FCT, 90010, Abuja, Nigeria.

[5] Mechanical Engineering Department, Lagos State University of Science and Technology, Ikorodu, 102222, Lagos State, Nigeria

* Corresponding Author: omiogbemi1@gmail.com TEL: (+234)-8037848496

Received: 02 October 2024; Accepted: 20 December 2024; Published: 31 December 2024
doi: 10.35934/segi.v10i2.113

Highlights:

- SMAW & GMAW analyzed at varied currents.
- GMAW caused coarse grains, weak strength.
- Weld hardness rose via martensite, pearlite.

Abstract: High-carbon steel, with a carbon content of 0.6% to 1.5%, is widely used in critical applications like cutting tools, springs, and high-performance bearings due to its strength, hardness and wear resistance. However, joining high carbon steel is challenging due to its susceptibility to cracking, brittleness, microstructural alteration in the heat affected zone. The impact of welding parameters, particularly current levels, on the mechanical and microstructural properties of high-carbon steel remains underexplored. This research explores the mechanical properties and microstructure of high-carbon steel welded using Shielded Metal Arc Welding (SMAW) and Gas Metal Arc Welding (GMAW) at varying current levels. SMAW was found to produce superior mechanical properties, with SMAW 140A achieving the highest ultimate tensile strength (495 MPa) and elongation (15%). In contrast, GMAW 120A had lower tensile strength (424 MPa) and elongation (10.5%). Higher current levels in GMAW, particularly GMAW 140A, resulted in coarser grain structures and reduced

mechanical performance, with a UTS of 317 MPa and elongation of 7.5%. Hardness testing revealed increased hardness in the weld zones of all samples, attributed to the formation of martensite and other hard phases such as pearlite and bainitic ferrite. Microstructural analysis via optical microscopy and SEM showed ferrite, pearlite, martensite, and bainitic ferrite, with SMAW samples displaying a lath martensitic structure and GMAW samples showing bainitic ferrite. These findings suggest that SMAW produces better mechanical properties and microstructural stability, making it more suitable for high-carbon steel applications requiring strength and durability.

Keywords: high carbon steel; SMAW; GMAW; mechanical properties; microstructure

1. Introduction

Steel is a widely used alloy primarily composed of iron and carbon, often enhanced with additional alloying elements to achieve specific mechanical properties and applications. High-carbon steels, characterized by carbon content ranging from 0.60% to 1.4%, are known for their hardness, strength, and wear resistance, making them ideal for applications such as cutting tools and springs (Ramadan *et al.,* 2023). However, their high carbon levels lead to challenges in welding, including susceptibility to cracking and loss of mechanical properties during the process. Tool and die steels often contain alloying elements like chromium and vanadium, which enhance their hardness through carbide formation. Despite their advantages, the difficulties in joining high-carbon steel necessitate careful consideration of welding techniques to maintain material integrity in critical applications (Callister *et.al.,* 2007).

The technique of joining the two workpiece surfaces to create a single product is called welding. Welding is a modern method of joining and creating different kinds of materials (Baskoro *et al.,* 2019). Welding is a common metal joining technique used in many industries, including aerospace, automotive, shipbuilding, and construction (Haider *et al.,* 2019). Shielded Metal Arc Welding (SMAW) is a welding process, also called “stick welding”, which is widely used in the construction industries and in repairing, as it offers more flexibility and portability. It makes use of a consumable electrode that has been covered in flux, a protective coating, to shield the joint. Shielding gas is released when the flux layer on the electrode begins to burn during welding, shielding the base metal and weldment from airborne contaminants. According to Quazi *et al.* (2019), the primary air pollutants that produce welding defects such as cracks and porosity are hydrogen and oxygen.

The Gas Metal Arc Welding (GMAW) process is a relatively complex process but is widely used in industry because of the speed at which joints can be made and the reliability of these joints in service (Tawfeek, 2017). Welding causes notable alterations to the mechanical characteristics, microstructure, and corrosion resistance of high-carbon steel. By applying heat and pressure, welding modifies the properties of the base material, which may have an impact on its hardness and strength (Shaalan *et al.,* 2019). Metallurgical processes such as recrystallization, phase changes, and solidification have an impact on the microstructure and can result in complicated stress patterns, embrittlement, and cracking (Husaini *et al.,* 2019). The final microstructure is greatly influenced by the temperature cycle during welding and the nature of the material, which frequently results in the development of ferrite, bainite, and martensite (Omiogbemi *et al.,* 2022).

Numerous research works have examined the impact of welding techniques on the microstructure and mechanical properties of high-carbon steel. Popović *et al.* (2006) analyzed high-carbon steel surface layers welded with self-shielded flux-cored wire, assessing mechanical and microstructural properties. Their findings revealed that transforming the original pearlitic structure into bainitic improved tensile strength, hardness, toughness, and fatigue resistance, making the repaired layers comparable to advanced bainitic steel. Kaewsakul *et al.* (2015) investigated the impact of gas metal arc welding (GMAW) parameters on penetration, microstructure, and hardness of AS3578-A350 steel (10 mm thick). They found that higher welding current (100-200A) and voltage (20-30 V) increased penetration depth, while slower welding speed (20-60 cm/min) further enhanced penetration. Shielding gases (Ar and Ar + CO_2) were also used. Afriansyah *et al.* (2024) compared SMAW and GMAW welding effects on carbon steel's microstructure, mechanical properties, and corrosion resistance. They found welding parameters influenced joint properties, with Vickers hardness testing, toughness evaluation, and SEM/EDS microstructural analysis highlighting differences. GMAW produced larger, more homogeneous grains, while SMAW resulted in coarser grains. Weld metal exhibited higher hardness due to precipitates like austenite and cementite, while the heat-affected zone had the lowest hardness, with fluctuations near the fusion line for SMAW. While extensive research has compared welding techniques like Shielded Metal Arc Welding (SMAW) and Gas Metal Arc Welding (GMAW) on carbon steel properties, a critical gap remains in understanding how microstructural transformations and precipitate distributions affect long-term performance under varying environmental and loading conditions. This study aims to fill this gap by exploring the relationship between microstructural characteristics and

mechanical performance in high-carbon steel applications. By optimizing welding methods, the research seeks to enhance mechanical performance, microstructural integrity, and long-term durability, providing valuable insights for improved engineering practices in industries that depend on high-carbon steel in diverse industrial applications.

2. Materials and Methods

2.1. Materials and Equipment

The material used in this study is a 12 mm thick High-carbon steel plate (AISI 1080) locally sourced from Kaduna State, Nigeria. Other materials were: electrode (E6013) of 3.2 mm, wire electrode (ER70S-6), Grinding disc (4-1/2" x 1/4 x 7/8" Model: T27), SiC abrasive paper grit. The equipment used were: GMAW Welding machine (Model: PANA-AUTO KRII500), SMAW welding machine (Model: Bx1-500), Lathe machine (Model: Harrison-M300), Grinding Machine (Model: A46-J-V), Scanning Electron Microscopy (Model: ThermoFisher Scientific Prisma E), Universal Tensile Testing Machine (Model: Instron 5900), Brinell Hardness Testing Machine (Model: Instron 5900).

2.2. Methods

The high carbon steel plate sample was machined to the specified dimensions: a gauge length of 40 mm, a thickness of 6 mm, a transition radius of 3 mm, and an overall length of 65 mm, utilizing a lathe machine in compliance with DIN 50125 standards. The procedure entailed securing the plate on the lathe and employing cutting tools to decrease the thickness from its original measurement to 6 mm and to trim the length to 40 mm. A chamfering tool was used to shape the 3 mm radius at the edges, and the overall length was machined finally to 65 mm. Finally, finishing operations like polishing or deburring ensure the sample meets the required dimensions and surface quality as shown in **Figure *1*.**

Figure 1. Tensile test sample

A 50 x100 mm weld pad was created by joining two 25 x 50 mm thick, 10 mm thick plates with one of their edges machined to a chamfered shape in order to test the hardness of the material in compliance with ASTM E10 standards. The welding methods used were SMAW and GMAW. SMAW was performed using an E6013 electrode with a diameter of 3.15 mm, operating at a voltage of 220 V and a current of 120 A and 140 A, utilizing a single V-groove weld design with DCEP polarity. For GMAW, a 2.5 mm diameter filler wire rod electrode was employed, also at a voltage of 220 V and a current of 120 A. The chemical composition of the high-carbon steel was analyzed using the X-ray fluorescence testing with the MAXx LMF14. This process involved identifying the key alloying elements present in the base metal sample during the X-ray fluorescence analysis. According to ASTM 2809, the first step in getting the sample ready for microstructural analysis is to cut it to the right size from the base metal using a rotary saw equipped with fine blades. The next phase was performing planar grinding using a standard abrasive grinding technique, beginning with 120 grits of course SiC paper and working down to 400 grits. using 1000 grit to finish. Subsequently, finer polishing is performed with MICROPAD-NAPPED high nap polishing pads. It has a very mild and delicate polishing action, and when used in conjunction with nital (a chemical etching solution made of 100 mL of ethanol and 1 mL of nitric acid), it can eliminate the minuscule grooves along the boundary that are visible under a microscope and create a new surface suitable for clear SEM analysis.

2.2.1. Tensile Test

The high-carbon steel samples were subjected to tensile tests in accordance with ASTM E8 Standard Method. These tests were carried out using the universal tensile testing machine (Model: Instron 5900) with a capacity of 20 kN. The high carbon steel samples were machined using a lathe machine into a standardized shape of the sample with a central reduced section for tensile test.

2.2.2. Hardness Test

The Brinell hardness testing method consists of indenting the test material with a hardened steel ball indenter, The hardened steel ball used in a Brinell hardness test is typically in the form of a spherical ball. The ball is made of hardened steel and comes in standard diameters, commonly 10 mm. During the test, the ball is pressed into the material surface under a load of 10 kg to create an indentation, which is then measured to determine the Brinell hardness number (BHN). The full load is normally applied for 15 seconds. Before the test, the mating surfaces of the indenter, plunger rod and the test samples were thoroughly cleaned by removing

the dirt, scratches, and oil. The test was carried out by adopting Omiogbemi *et al.* (2022) method.

2.2.3. Optical Microscope and Scanning Electron Microscope of High Carbon Steel

The welded and the non-welded high carbon steels were viewed using an optical microscope and scanning electron microscope (SEM) with a magnification between 50x to 500x. The samples for investigation were prepared according to the specifications of the machine as adopted by Omiogbemi *et al.* (2023). The setup was then loaded into the column which is connected to the monitor in a closed loop for which control and feedback are actualized.

3. Results and Discussion

The chemical composition of steel was determined using the X-ray fluorescence (XRF) and is given in **Table *1***.

Table 1. Chemical composition of the parent metal

Element	C	Si	P	Cr	Mn	S	Ni
Concentration (wt. %)	1.33	0.99	0.03	0.05	1.64	0.209	4.86
Element	Cu	V	W	La	Zn	Co	Fe
Concentration (wt. %)	0.74	0.52	0.196	0.160	0.03	0.10	89.145

3.1. Tensile Test Properties of High Carbon Steel

Figure *2* depicts the variation of force against the extension of the tensile test of the weldment of high-carbon steel of the different welding processes. It was observed generally that with a gradual increase in load, there is a corresponding increase in extension of the specimen; that is the extension produced is directly proportional to the load of which the trend of the result of the tensile analysis of the welded samples corresponds with the findings of Omiogbemi *et al.* (2017) on his study of the effect of metal inert gas welding parameters on some mechanical properties of austenitic stainless steel in an acidic environment. This continues until the maximum load is reached. At this point of maximum load, a neck is produced. The smaller area was not able to resist the strain being applied, consequently, the specimen finally cracked at this new location which is called the breaking load point. For sample 1 (Control) the UTS was 689 MPa, the yield strength was 618 MPa and the percentage elongation was 17.5%. For sample 2 (SMAW 120A) the UTS was 459 MPa, the Yield Strength was 406 MPa and the percentage elongation was 10%. For sample 3 (SMAW 140A) the UTS was 495 MPa, the yield

strength was 406 MPa and the elongation was 15%. For sample 4 (GMAW 120 A) the UTS was 424 MPa, the yield strength was 389 MPa, and the percentage elongation was 12.5%. For Sample 5 (GMAW 140 A) the UTS was 317 MPa, the yield strength was 265 MPa and the percentage elongation was 7.5%. Based on the data obtained, it was observed that the ultimate tensile strength, yield strength and elongation values of the base metal was higher compared to the welded specimens due to its uniform microstructure. Among the welded samples, the samples welded with SMAW at 140 A and GMAW at 120 A displayed the highest values of ultimate tensile strength, yield strength and elongation as shown in **Figure *2*.**

The results of the present study show that sample 3 (SMAW 140 A) provide better mechanical properties than Sample 2 (SMAW 120 A), Sample 4 (GMAW 120 A) and Sample 5 (GMAW 140 A). This suggests that this sample can endure more stress compared to Sample 2 (SMAW 120 A), Sample 4 (GMAW 120 A) and Sample 5 (GMAW 140 A). This phenomenon is associated with the higher current and voltage in gas metal arc welding, which raises the heat input during the welding process. The increased heat input results in the formation of a larger weld pool and a wider heat-affected zone, both of which take longer to cool and dissipate heat. Consequently, the observed drop in mechanical characteristics shows that larger current values decrease tensile strength due to slow cooling rates, where SMAW uses a flux-coated consumable electrode, resulting in lower heat input compared to GMAW, and is influenced by the welder's skill.

The slag layer formed over the weld pool moderates the cooling process, acting as an insulator that slightly slows cooling while still allowing for faster cooling than GMAW. This slag protects the weld from oxidation, controls the cooling rate, and minimizes thermal stresses. The smaller weld pool cools and solidifies more quickly, promoting finer grains in the heat-affected zone (HAZ), which enhances tensile strength and toughness while reducing the risk of hot cracking and other defects. In contrast, GMAW employs a consumable wire electrode and shielding gas (argon) to protect the weld pool from atmospheric contamination. Its high current and voltage generate significant heat input, creating a large weld pool and an extensive HAZ. The absence of cooling assistance from the shielding gas results in slower cooling rates, allowing for coarse grain growth in the HAZ, which reduces toughness and tensile strength. Additionally, welding faults tend to grow at higher current values as agreed by Pandey *et al.* (2021); Omiogbemi *et al.* (2021) and Omiogbemi *et al.* (2022).

The mechanical properties observed in this study were correlated with the microstructural features revealed in SEM micrographs in **Figure *5* and Figure *6***, highlighting the role of

microstructural integrity in determining material performance as opined by Smith and Johnson (2022) and Lee *et al.* (2023).

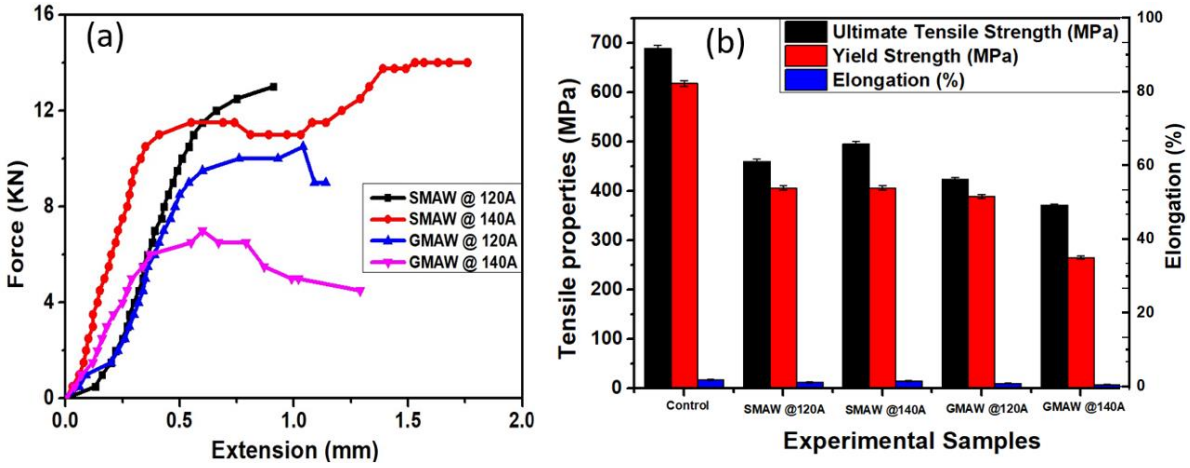

Figure 2. Tensile test analysis: (a) force vs extension of welded samples with SMAW and GMAW at currents of 120 A and 140 A and (b). tensile properties of control and welded samples with SMAW and GMAW at currents of 120 A and 140 A

3.2. Hardness Properties of High Carbon Steel

Figure *3*. illustrates the hardness values obtained from both sides of the sample transversely for the different samples welded by SMAW and GMAW. The hardness value is higher in the GMAW samples while for the SMAW sample, there was in reduction in the hardness value welded zone. This could be due to the formation of martensite caused by the heat generated during welding which is consistent with the observation made by Owolabi *et al.* (2016) and Omiogbemi *et al.* (2022) where it was stated that the hardness increased purely due to the distortion of the grain size and formation of martensite or bainite in the weldments when heat is applied. The hardness value at the welded zone increased because of the cooling rate the austenite phase changed into martensite. The martensite is a hard and brittle phase due to its distorted crystal structure (body-centered tetragonal structure), which results from the high carbon content being trapped in solution during the transformation as indicated by Sou (2015).

3.3. Optical Microscopy and Scanning Electron Microscope of High Carbon Steel

Figure *4*(a) and **Figure *4*(b)** display the optical micrographs of the samples at magnifications of 100x and 50x, respectively. The analysis reveals a striking microstructure that distinctly illustrates the proportions of ferrite and pearlite (ferrite and cementite) phases within the steel. The dark regions signify pearlite, which overwhelmingly dominates the structure, while the lighter ferrite occupies a smaller volume fraction and exhibits no discernible alignment with

the original austenite grains from which it formed. This observation unequivocally confirms the classification of the steel as high carbon. Moreover, these findings are consistent with the research conducted by Tarif Tawfeek *et al.* (2016), which explored the impact of GMAW parameters on both the welded zone and heat-affected zone of steel, further validating the significance of microstructural analysis in understanding material properties.

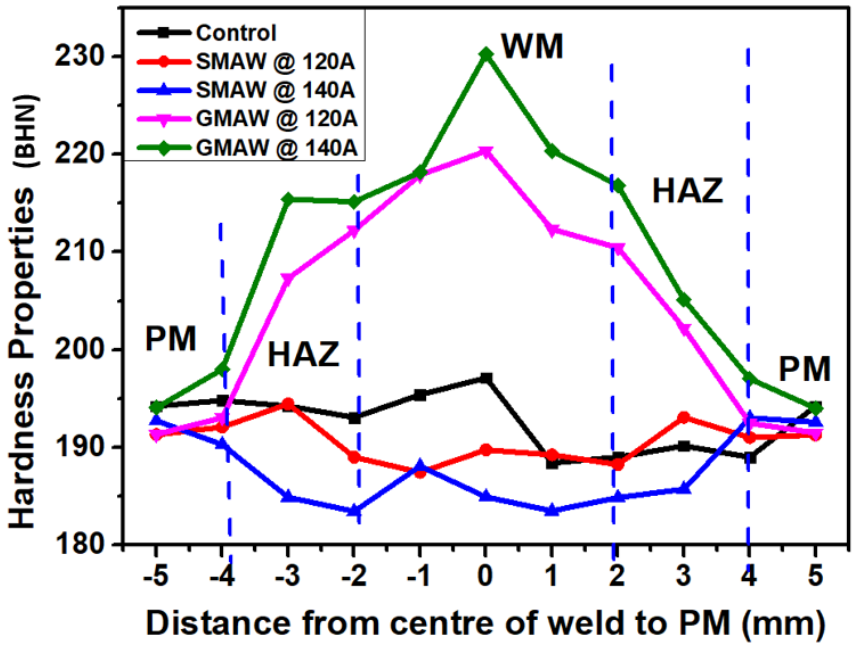

Figure 3. The hardness analysis taken from the centre of the weld to the parent metal using SMAW and GMAW at currents of 120 A and 140 A

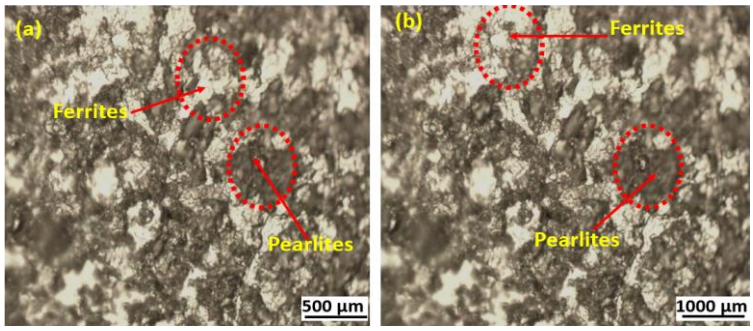

Figure 4. Optical micrograph of parent metal

The SEM micrographs of the parent metal sample, captured at magnifications of 100x, 250x, 500x and 1000x are presented in **Figure *5*.** These images provide critical insights into the microstructure of the base metal prior to welding, revealing a composition characterized by ferrite (light areas) and pearlite (dark areas), both of which exhibit a fine grain size due to previous thermomechanical treatment. This analysis is closely aligned with the research conducted by Hasan *et al.* (2020), which explores the role of prior bainite/martensite phases in

the microstructure of TRIP steel. The intricate details observed in these micrographs underscore the complex interplay of phases that contribute to the material's overall properties, highlighting the importance of understanding microstructural evolution in advanced high-strength steels. The fine-grained ferrite and pearlite microstructure observed in SEM micrographs enhances the material's toughness, tensile strength, and ductility, demonstrating the critical influence of microstructural evolution on mechanical performance as corroborated by some researchers (Hasan *et al.,* 2020; Zhao *et al.,* 2021).

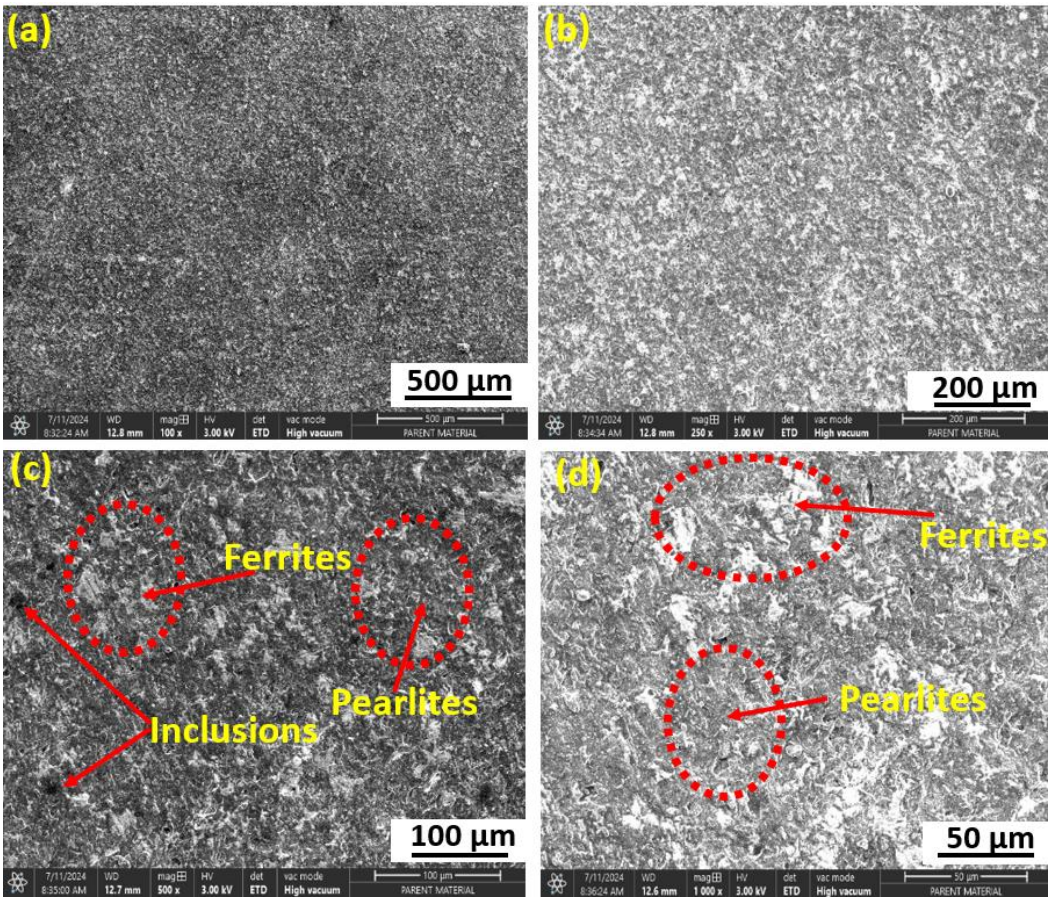

Figure 5. SEM micrograph of parent metal sample

Figure *6*(a) and **Figure *6*(c)** present SEM micrographs of SMAW and GMAW samples at varying magnifications (100x and 500x), respectively and **Figure *6*(b) and Figure *6*(d)** present SEM micrographs of GMAW, samples at varying magnifications (250x and 1000x), respectively, revealing distinct microstructural characteristics. In the SMAW sample, the high hardenability of high-carbon steel, coupled with the decomposition of micro-alloyed carbides during welding, leads to coarse-grained formations in the fusion zone. This process generates a lath martensitic microstructure with retained austenite, aligning with findings on residual austenite and martensitic transformation in steel reported by Mostafapour and Saeid (2016). In

contrast, the GMAW sample exhibits a bainitic ferrite microstructure interspersed with retained austenite and martensitic-austenitic zones. This variation highlights the critical influence of transformation temperatures and cooling rates, corroborating studies by Mostafapour and Saeid (2016), Tawfeek *et al.* (2016), and Hasan *et al.* (2020). These insights underscore the intricate relationship between microstructural evolution and thermal dynamics during welding.

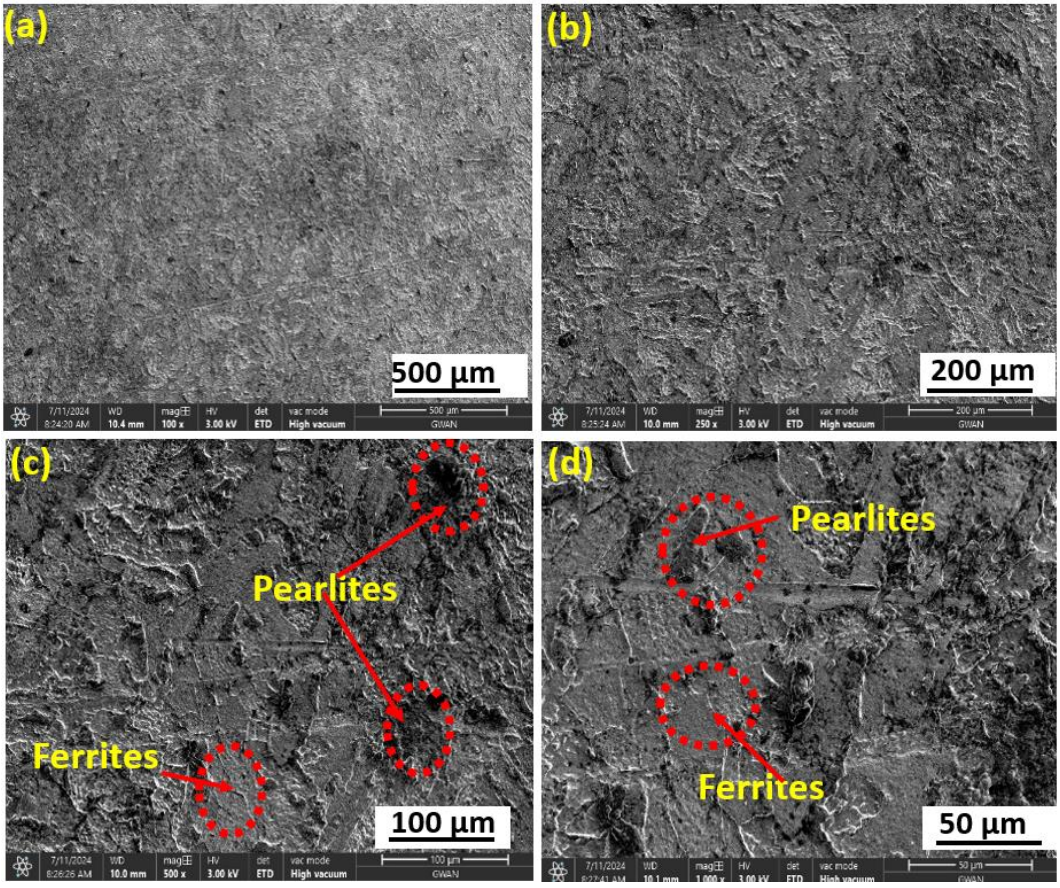

Figure 6. SEM micrograph of SMAW and GMAW sample

4. Conclusion

The study compared Shielded Metal Arc Welding (SMAW) and Gas Metal Arc Welding (GMAW) techniques. Results showed that SMAW produced materials with higher ductility and ultimate tensile strength (UTS) than GMAW. Specifically, SMAW 140A demonstrated the highest UTS (495 MPa) and elongation (15%), outperforming GMAW 120A (UTS: 424 MPa, elongation: 10.5%). Higher currents, particularly in GMAW, led to coarse grains and rapid cooling, compromising weld strength and ductility. All welded samples exhibited increased hardness in weld zones due to rapid cooling and carbon alloying, promoting hard phases like martensite. Optical microscopy revealed the steel's microstructure consisted mainly of pearlite

with minimal ferrite, characteristic of high-carbon steel. The base metal's initial microstructure was stable and homogeneous, with fine-grained pearlite and ferrite.

Acknowledgement

The authors would like to thank the Mechanical Engineering Department, Air Force Institute of Technology (AFIT), Nigerian Air Force Base, Kaduna for supporting the research and, the Nigerian Defence Academy (NDA) for availing their equipment for some of the analysis.

Credit Author Statement

Supervision and correction of drafted manuscript, Omiogbemi, I.M.B.; Conceptualization and methodology, Omiogbemi, I.M.B., Olatunji, E.C., Awopetu, G.A., Awwal, K.S.; investigation, Olatunji, E.C., Awopetu, G.A., Awwal, K.S.; writing—original draft preparation, Olatunji, E.C., Awopetu, G.A., writing—review and editing, Omiogbemi, I.M.B., Awode, E.I, Okwum, C., Inobeme, F.O., Dagwa, M.I.

Conflicts of Interest

No potential conflict of interest was disclosed by the authors.

References

Abioye, T. E., Folorunso, D. O., & Samuel, O. D. (2019). Optimization of Process Parameters of TIG Welding of Stainless Steel 304. *Materials Research Express, 6*(9). https://doi.org/10.1088/2053-1591/ab2f95

Afriansyah, Z., Ashof, M., & Naimah, A. (2024). Comparison of SMAW and GMAW welding properties. Mechanics Exploration and Material Innovation, 1(2), 48–53. Retrieved from https://memi.ub.ac.id/index.php/memi

ASTM E10-18, (2018). Standard Test Method for Brinell Hardness of Metallic Materials. ASTM International.

ASTM E3-11, (2011). Standard Guide for Preparation of Metallographic Specimens. ASTM International.

ASTM E2809-22, (2022). Standard Guide for Scanning Electron Microscopy (SEM) Testing of Metallic and Nonmetallic Materials. ASTM International.

Baskoro, A. S., Putra, D. U., & Rumbiak, D. B. (2019). The Effect of Welding Parameters on Microstructure in Dissimilar Welding of Stainless Steel 316L and Structural Steel on Gas Metal Arc Welding (GMAW).Ad

Bhaduri, A. K., Rai, S. R., & Kumar, V. (2015). Developments in Joining of Advanced High-Strength Steels for Automotive Applications. Welding Journal, 94(1), 1–12. https://doi.org/10.29391/2023

Biodun Owolabi, O., Christopher Aduloju, S., Sobechukwu Metu, C., Ebele Chukwunyelu, C., & Charles Okwuego, E. (2016). Evaluation of the Effects of Welding Current on Mechanical Properties of Welded Joints Between Mild Steel and Low Carbon Steel. American Journal of Metallurgical and Materials Engineering, 1(1). Retrieved from http://www.openscienceonline.com/journal/ajmme

Callister, W. D., & Rethwisch, D. G. (2007). Materials Science and Engineering: An Introduction (7th ed.). John Wiley & Sons.

DIN 50125:2020-03: Testing of metallic materials - Tensile test pieces. Deutsches Institut für Normunge.V. (DIN).

Gao, X., Zhang, Y., & Wang, L. (2018). Effect of Welding Speed on Microstructure and Mechanical Properties of TIG Welded High-Strength Steel Joints. Journal of Manufacturing Processes, 33, 217–225. https://doi.org/10.1016/j.jmapro.2018.05.011

Haider, S. F., Quazi, M. M., Bhatti, J., Nasir Bashir, M., & Ali, I. (2019). Effect of Shielded Metal Arc Welding (SMAW) parameters on mechanical properties of low-carbon, mild, and stainless-steel welded joints: A review. *Journal of Advances in Technology and Engineering Research, 5(5). https://doi.org/10.20474/jater-5.5.1

Hasan, S. M., Kumar, S., Chakrabarti, D., & Singh, S. B. (2020). Understanding the effect of prior bainite/martensite on the formation of carbide-free bainite. Philosophical Magazine, 100(7), 797–821. https://doi.org/10.1080/14786435.2020.1712486

Hasan, M. A., Ahmed, K., & Rahman, M. (2020). Influence of microstructural phases on the mechanical properties of TRIP steel. Journal of Materials Science & Technology, 37(5), 843-856. https://doi.org/10.1016/j.jmst.2019.10.021

Kaewsakul, N., Putrontaraj, R., &Kimapong, K. (2015). The effects of GMAW parameters on penetration, hardness, and microstructure of AS3678-A350 high strength steel. International Journal of Advanced Culture Technology, 3(1), 169-178.

Lee, J., Kim, H., & Park, S. (2023). Influence of microstructural characteristics on mechanical properties of polymer composites. Journal of Composite Materials, 57(3), 345–358.

Mostafapour, A., Ebrahimpour, A., & Saeid, T. (2016). Identification of Retained Austenite, Ferrite, Bainite, and Martensite in the Microstructure of TRIP Steel. International Journal of ISSI, 13(2).

Omiogbemi, I.M.B., Yawas, D.S., Das, A. Afolayan, M.O., Dauda, E.T., Kumar, R. & Chowdhury, S.G (2023). Effect of electrode configuration on the mechanical-corrosion characteristics of welded

AISI 2205 steel structure. MRS Advance, 8(9), 499-507. https://doi.org/10.1557/s43580-022-00489-8

Omiogbemi, I.M.B., Yawas, D.S., Das, A. Afolayan, M.O., Dauda, E.T., Kumar, R., Gorja, S.R. & Chowdhury, S.G (2022). Mechanical properties and corrosion behaviour of duplex stainless-steel weldment using novel electrodes. Sci Rep. 12, 22405. https://doi.org/10.1038/s41598-022-26974-6.

Omiogbemi, I.M.B., Faci, D.N., Gummadi, K.A., Negash, M.S., Sardar, B., Gad, M.S., Dagwa, M.I. & Audu, T.S. (2022). The influence of the arc welding process on the mechanical and microstructural characteristics of low carbon steel in a corrosive environment. Macromolecular Symposia, 402(1), https://doi.org/10.1002/masy.202100362.

Omiogbemi, I.M.B., Yawas, D.S., Afolayan, M.O. & Dauda, E.T. (2021). Effect of welding conditions and flux compositions on the metallurgy of welded duplex stainless steel. Materials Today: Proceedings, Vol.49,1162-1168. https://doi.org/10.1016/j.matpr.2021.06.161.

Omiogbemi, I.M.B., Yawas, D.S., Dagwa, I.M., & Okibe, F.G. (2017). Effects of Metal Inert Gas Welding Parameters on Some Mechanical Properties of Austenitic Stainless Steel in Acidic Environment. Nigerian Journal of Technology, 36(3), 835–843. https://doi.org/10.4314/njt.v36i3.25

Pandey, P. K., Ramteke, S., Kumar, A., Meena, S., & Rana, V. (2021). A Review on Welding Characteristics of Ferritic Stainless Steels and Effects of Various Weld Process Parameters. JETIR, Vol. 8. www.jetir.orga559.

Popović, O., Prokić-Cvetanović, R., Grabulov, V., Odanović, Z. (2006). Selection of flux-cored wires for surfacing railway tracks, Welding and Welded Structures, 4/2006. pp.131-139.

Ramadan, N., Embaia Almabrouk, M. M., Mahdi, H., & Naser, E. (2023). Online (2790-5721)-Print (2790-5713) .In Surman Journal for Science and Technology .

Sanjurjo, E., & Fernández-Abia, A. (2020). Influence of Heat Input on Microstructure and Mechanical Properties of Welded Joints in S355 Structural Steel. Metals, 10(3), 357. https://doi.org/10.3390/met10030357

Shi, X., Zhang, W., & Luo, Y. (2017). Microstructure and Mechanical Properties of Dissimilar Metal Welds Between Low Alloy Steel and Stainless Steel. Materials Characterization, 131, 273–280. https://doi.org/10.1016/j.matchar.2017.07.005.

Smith, R., & Johnson, T. (2022). SEM analysis and its correlation with mechanical behavior in advanced materials. Materials Science and Engineering A, 845, 112345.

Tawfeek, T. (2017). Study the Influence of Gas Metal Arc Welding Parameters on the Weld Metal and Heat Affected Zone Microstructures of Low Carbon Steel. International Journal of Engineering and Technology, 9(3), 2013–2019. https://doi.org/10.21817/ijet/2017/v9i3/1709030272.

Zhao, Y., Wang, L., & Liu, J. (2021). Effects of bainite/martensite phases on the mechanical properties of advanced high-strength steels. Materials Science and Engineering: A, 810, 141286. https://doi.org/10.1016/j.msea.2021.141286